PERGAMON

Deep-Sea Research I 46 (1999) 545–572

DEEP-SEA RESEARCH
PART I

Reconciling thermodynamic and dynamic methods of computation of water-mass transformation rates

John Marshall*, Daniel Jamous, Johan Nilsson[1]

Program in Atmospheres, Oceans and Climate, Department of Earth, Atmospheric and Planetary Sciences, Massachusetts Institute of Technology, RM. 54-1526, Cambridge, MA 02139-4307, USA

Received 19 September 1997; received in revised form 24 February 1998; accepted 14 May 1998

Abstract

The computation of the water-mass transformation rate in a particular density range from thermodynamic and dynamic methods are compared and reconciled by diagnosis of the Atlantic sector of a global integration of an ocean model driven by analyzed air–sea fluxes. In the absence of diffusive processes, the rate of subduction of fluid between two density surfaces across a fixed control surface, and integrated across the ocean from one solid boundary to another, must be equal to the rate of formation of fluid at the sea surface induced by surface fluxes in that density range. But due to the action of mixing on the body of fluid between the control surface and the sea-surface, transformation may differ from the integrated subduction. We find that vertical diffusive fluxes at the base of the winter mixed layer and in the seasonal thermocline can substantially modify transformation due to air–sea interaction and bring about an accommodation between it and the subduction rate. In high latitudes, an additional accommodation is achieved by lateral diffusive fluxes directed across the almost vertical isopycnals, typical of the deep, end-of-winter mixed layers of the sub-polar gyre. Finally we speculate on the likely nature and intensity of the mixing processes at work in the boundary layer of the ocean and their role in subduction and transformation.

1. Introduction

The ocean can be imagined to consist of layers of fluid stacked one on top of the other. As the ocean circulates, the layers tilt relative to the horizontal, and some

* Corresponding author. Fax: 1 617 253 4464; e-mail: marshall@gulf.mit.edu

[1] Current address: Department of Meteorology, University of Stockholm, S-10691 Stockholm, Sweden.

0967-0637/99/$ – see front matter
PII: S0967-0637(98)00082-X

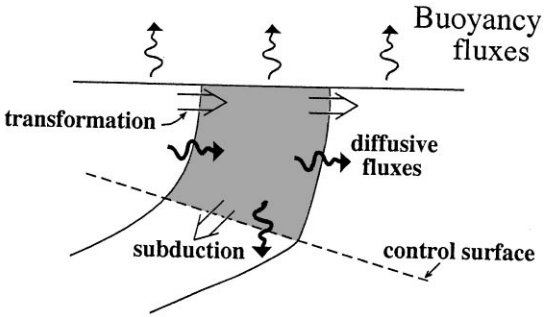

Fig. 1. A schematic diagram of the upper ocean showing the sea surface, two outcropping isopycnals and a fixed control surface across which the subduction is monitored. Buoyancy fluxes at the sea surface and diffusive fluxes in the interior transform water masses from one density class to another. We will be interested in those processes associated with changes in the volume of the shaded fluid, which resides between the sea surface and the control surface.

outcrop at the sea-surface, providing a pathway in to the interior — see Fig. 1. In the main thermocline the water-mass properties and density of the layers are relatively constant, but they are changed — transformed — when exposed directly to mechanical and thermodynamic forcing in the upper boundary layer of the ocean.

Patterns of heating/cooling, precipitation/evaporation and mechanical stress associated with the prevailing winds induce a cycle of mixing (by convection, mechanical stirring and myriad other processes) and restratification, which changes the volume and water-mass properties of the surface layers. Fluid is carried by the large-scale circulation and passes to and from this seasonal boundary layer. Quantities of great interest and climatological importance are:

(I) *The formation rate*: Fluid passes laterally across outcropping isopycnals at the sea surface; the convergence of this *transformation* flux yields the formation rate, the rate at which fluid that makes up a particular layer is created or destroyed by air–sea fluxes (see Fig. 1). Walin (1982), Speer and Tziperman (1992) and Garrett et al. (1995) have made important contributions to the quantification of the transformation rate both theoretically and observationally.

(II) *The subduction rate*: The rate at which fluid passes between the seasonal boundary layer of the ocean and the ocean's interior — see Fig. 1. Subduction has been defined and the physical processes controlling it discussed in, for example, Stommel (1979), Marshall and Nurser (1992), Marshall et al. (1993) and Huang and Qiu (1994). It is of interest because the mixed layer acts as a rectifier of the highly variable meteorological force acting at its upper surface, only transmitting seasonally biased properties through to the thermocline below (see Williams et al., 1995).

Formation and subduction are clearly related to one another but are different in important and subtle ways; the former is an integral statement about the rate of creation (and destruction) of water masses at the sea–surface by air–sea interaction.

The latter is a local statement about the flux of fluid within a certain density range between the mixed-layer and the stratified interior.

This article has two main purposes. The first is a pedagogical one — formation and subduction are discussed in one framework using a common nomenclature and we attempt to clearly expose their connections and differences. Many of the formulae have, in various forms, been written down before, but the literature on "subduction" and "transformation" has, hitherto, been quite separate and the common links between them not described. The subduction of fluid between two density surfaces, integrated across the ocean from one coast to the other, is equal to the formation driven by air–sea fluxes, if there are no diffusive processes acting on the volume of fluid shaded in Fig. 1. (see Speer et al., 1995). Our ideas are illustrated by appropriate diagnosis of the Atlantic sector of a global integration of the MIT ocean model (Marshall et al., 1997a, b) forced with analyzed air–sea fluxes.

Our second purpose is to reconcile, at least in the context of this numerical model, computations of water mass transformation from the different perspectives provided by the thermodynamic method (I above) and the dynamic method (II above). Studies from data (see, for example Speer, 1997) have suggested that there may be a large discrepancy between the two methods leading to speculation on mixing processes that need to be invoked to bring about a reconciliation (see the note by Tandon and Garrett, 1997 and the paper by Garrett and Tandon, 1997). For example Tandon and Garrett note that between $\sigma = 23$ and $\sigma = 26$ in the North Atlantic, estimates of formation rates from air–sea fluxes using thermodynamic and dynamic methods are of different sign and disagree by at least 14 Sv. Here it is argued that vertical diffusive fluxes—at the base of the winter mixed layer and in the seasonal thermocline—substantially modify transformation due to air–sea interaction and bring about an accommodation between it and the subduction rate. At high latitudes, an additional accommodation is achieved by diffusive fluxes directed laterally across the almost vertical isopycnals of deep, end-of-winter mixed layers typical of the North Atlantic sub-polar gyre. Although reliance is placed on insights gained from a numerical model, we believe that our broad conclusions transcend that particular model and are relevant to the real ocean. We focus on the Atlantic so that our results can be readily compared to previous calculations — for example those of Speer and Tziperman (1992) and Nurser et al. (1998), so building confidence in our methods and models. It should be mentioned that the latter study, as here, presents calculations from a numerical model (using the Miami isopycnal ocean model coupled to a Kraus–Turner mixed layer model), but in Nurser et al. (1998), diagnostics are performed over entire isopycnal layers. Here, by considering the region limited by the sea surface and the base of the winter mixed layer, we are able to focus explicitly on the relationship between subduction rates and formation rates induced by air–sea fluxes.

The paper is set out as follows. In Section 2 the kinematics and in Section 3 the thermodynamics of water-mass transformation are discussed using a common nomenclature and drawing out the connections between them. These sections are rather general. In Section 4 we diagnose a numerical model — that of Marshall et al. (1997a, b) — to ascertain the various processes at work in determining the rates of

subduction and transformation. Finally, in Section 5 we attempt to draw some general conclusions that are pertinent to the real ocean.

2. The kinematics of water-mass transformation

2.1. The volume flux in to the main thermocline

Define a fixed Eulerian surface, $z = -H(x, y)$, across which we wish to compute the flux of properties to and from the main thermocline (see Fig. 2a). In practice H may be chosen to be any convenient surface, such as the depth of the winter mixed-layer or the top of the main thermocline. But whatever surface we choose, it is kept fixed in time. The subduction rate, the volume flux across the surface, is given by (e.g. Marshall et al., 1993):

$$S(x, y, t) = -\mathbf{v}_H \cdot \nabla H - w_H \tag{2.1}$$

$\mathbf{v}_H$ and w_H are the horizontal and vertical velocity components at the depth H, respectively. S is positive if there is flow across H in to the thermocline. By assuming the thermal wind relation and adopting a level of no motion to estimate $(\mathbf{v}_H, w_H)$, Eq. (2.1) allows one to estimate the subduction rate across the winter mixed-layer base

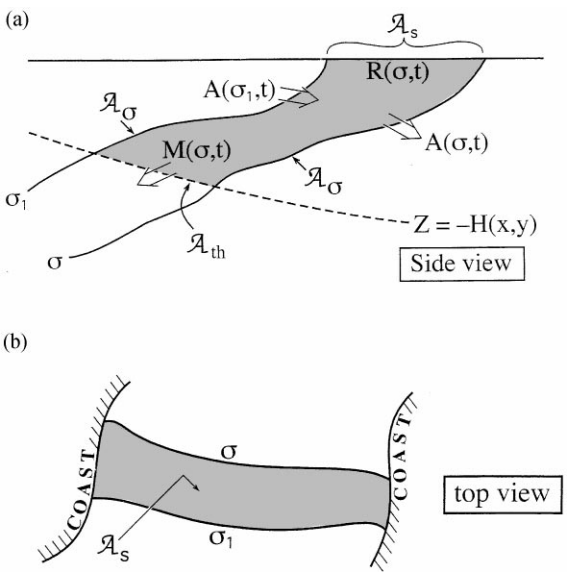

Fig. 2. The shaded fluid $R(\sigma, t)$ is circumscribed by isopycnal surfaces laterally and, vertically, by a fixed surface $H(x, y)$ and the sea-surface. These surfaces have areas $\mathcal{A}_\sigma(\sigma, t)$, $\mathcal{A}_\sigma(\sigma_1, t)$ $\mathcal{A}_{th}(\sigma, t)$ and $\mathcal{A}_S(\sigma, t)$. The diapycnal volume fluxes through the isopycnal surfaces is $A(\sigma, t)$ and the volume flux across $H(x, y)$ in to the interior of the ocean is M. (b) The fluid volume $R(\sigma, t)$ outcrops at the sea surface with a window of area $\mathcal{A}_S(\sigma, t)$.

from observations of the hydrography and Ekman pumping; a discussion of the procedure is given by Marshall et al. (1993).

A related quantity, which we shall call $M(\sigma, t)$, is the *net* volume flux across the surface $H(x, y)$ in to the thermocline in the density interval from σ_1 to σ, integrated across an ocean basin (see Fig. 2b). Here σ_1 is a conveniently chosen reference density taken to be less than σ:

$$M(\sigma, t) = \iint_{\mathscr{A}_{\rm th}(\sigma,t)} S(x, y, t)\, \mathrm{d}\mathscr{A}', \quad \mathrm{d}\mathscr{A}' \equiv \frac{\mathrm{d}\mathscr{A}}{\sqrt{1 + (\nabla H)^2}}. \tag{2.2}$$

where $\mathrm{d}\mathscr{A}$ is an element of area on $\mathscr{A}_{\rm th}(\sigma, t)$, and $\mathrm{d}\mathscr{A}'$ is the projection of $\mathrm{d}\mathscr{A}$ on the horizontal plane (note that generally $\mathrm{d}\mathscr{A} \approx \mathrm{d}\mathscr{A}'$).

The region $R(\sigma, t)$ sketched in Fig. 2, extends laterally over the whole ocean basin and terminates at coastal boundaries; it is bounded above by the sea surface, below by the surface $z = -H(x, y)$, and laterally by two surfaces of constant density, $\sigma(\mathbf{x}, t) = \sigma$ and $\sigma(\mathbf{x}, t) = \sigma_1$, respectively. The surfaces that bound R are labelled: $\mathscr{A}_\sigma(\sigma, t)$, $\mathscr{A}_{\rm th}(\sigma, t)$, $\mathscr{A}_\sigma(\sigma_1, t)$ and $\mathscr{A}_{\rm S}(\sigma, t)$.

The quantity

$$\delta M = \frac{\partial M}{\partial \sigma}\, \delta\sigma \tag{2.3}$$

is the volume flux in to the main thermocline in the infinitesimal density-band between σ-dσ and σ. It should be noted that even when $\partial M/\partial\sigma$ is zero the surface layer and the thermocline can exchange fluid locally, i.e. S may not be locally zero; however the *net* exchange over the density interval vanishes if $\partial M/\partial\sigma$ is zero.

2.2. The volume budget of the surface layer

The volume of R, say $V(\sigma, t)$, is altered only by the volume fluxes across the boundaries of R. Ignoring volume fluxes across the sea floor and the sea surface, conservation of the volume of R can be expressed thus:

$$\frac{\partial V(\sigma, t)}{\partial t} = A(\sigma_1, t) - A(\sigma, t) - M(\sigma, t). \tag{2.4}$$

Here A denotes the net diapycnal volume flux through the isopycnal surface $\mathscr{A}_\sigma(\sigma, t)$; A is counted positive for flow towards increasing density, i.e. typically to the north. Note that in Eq. (2.4), boundary mass-sources such as exchange with adjacent ocean-basins have been neglected. In the North Atlantic, for example, cross-equatorial exchange could give non-negligible contributions to the volume of R in certain density ranges.

By taking the derivative of Eq. (2.4) with respect to the density, we obtain the mass budget for the infinitesimal volume of the surface layer between the isopycnal surfaces σ-dσ and σ:

$$\frac{\partial^2 V(\sigma, t)}{\partial t\, \partial\sigma} = -\frac{\partial A(\sigma, t)}{\partial\sigma} - \frac{\partial M(\sigma, t)}{\partial\sigma}. \tag{2.5}$$

Note that the reference density σ_1, which is an integration constant, does not appear in Eq. (2.5). Furthermore, if σ_1 is interpreted as σ-dσ, then Fig. 2 portrays this infinitesimal region; its volume is changed by divergence, with respect to density, of the cross-isopycnal flow and flux across H.

2.3. *The seasonal cycle and the annually averaged subduction*

Over the subtropical and sub-polar gyres, variations in surface buoyancy-flux drive the seasonal thermocline and the mixed layer through a pronounced annual cycle. Fig. 3 sketches schematically the evolution of the region R with the seasons as outcrops sweep first north and then south. At some point in the late winter, when the outcrops reach their southern most limit, V attains its minimum value. This instant occurs between March and April in the subtropical gyre (see Marshall et al., 1993). As the year progresses, the surface buoyancy-flux forces the volume of R to increase as the outcrops extend northwards, and then decrease again to return to the winter positions.

The annual cycle of the surface layer permits us to make some simplifications when the annually averaged subduction $\overline{M}(\sigma)$, say, is sought. If we assume that there is no interannual variability, the rate of change of V vanishes when averaged over a year and then from Eq. (2.4), the annual subduction is determined by the annual value of the cross isopycnal flow:

$$\boxed{\overline{M}(\sigma) = \bar{A}(\sigma_1) - \bar{A}(\sigma)}\,. \tag{2.6}$$

From Eq. (2.6) we note that

$$\frac{\partial \bar{A}}{\partial \sigma} = -\frac{\partial \overline{M}}{\partial \sigma} \tag{2.7}$$

and so, from Eq. (2.3),

$$\delta \bar{A} = -\delta \overline{M}$$

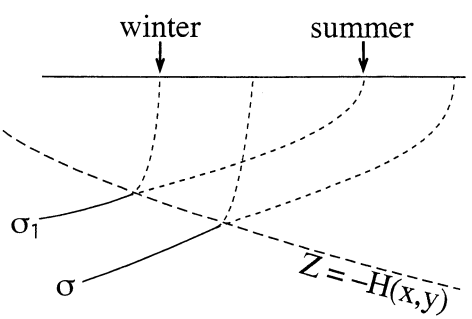

Fig. 3. Schematic diagram showing the migration of the outcrops from their summer to their winter positions.

where $\delta\overline{M}$ is the volume flux between σ and σ-dσ. Eqs. (2.3) and (2.7) tell us, in principle at least, how one might compute the diapycnal volume flux A from M, which is itself computable from S, using Eq. (2.2). Note that A is the *diapycnal* volume flux and so is intimately tied to thermodynamics (see Section 3). But it is also related to M, and hence S, through kinematics.

3. The thermodynamics of water-mass transformation

3.1. The buoyancy budget

The foregoing discussion was concerned entirely with definitions and kinematics. However, Walin (1982) showed that the diapycnal volume flux A is intimately tied to the buoyancy budget of R: buoyancy has to be supplied to allow water to cross isopycnal surfaces, and if this association is made quantitative, a relation of diagnostic value results.

Consider the continuity and buoyancy equations:

$$\nabla\cdot\mathbf{v} = 0 \tag{3.1}$$

$$\frac{\partial\sigma}{\partial t} = -\nabla\cdot(\mathbf{N}_\sigma + \sigma\mathbf{v}). \tag{3.2}$$

Here $\mathbf{v}$ is the fluid velocity, $\mathbf{N}_\sigma$ is the non-advective flux of potential density and $\sigma\mathbf{v}$ the advective flux. In the following the divergence of $\mathbf{N}_\sigma$ will be referred to as the buoyancy forcing. We make the reasonable assumption that the normal components of $\mathbf{v}$ and $\mathbf{N}_\sigma$ vanish at the sea floor. At the sea surface, the normal component of the velocity is also set to zero.

The diapycnal volume flux, A, is the flux through an isopycnal surface; that surface may move through the fluid at a velocity different from the fluid velocity. Now the velocity of an isopycnal surface normal to itself, say $\mathbf{v}_\sigma$, is given by

$$\mathbf{v}_\sigma \equiv -\hat{\mathbf{n}}_\sigma(\partial\sigma/\partial t)/|\nabla\sigma|, \quad \hat{\mathbf{n}}_\sigma \equiv \nabla\sigma/|\nabla\sigma|$$

To calculate the volume flow across $\mathscr{A}_\sigma(\sigma, t)$, we must accordingly subtract $\mathbf{v}_\sigma$ from the Eulerian fluid velocity, that is

$$A(\sigma, t) = \iint_{\mathscr{A}_\sigma(\sigma,t)} (\mathbf{v} - \mathbf{v}_\sigma)\cdot\hat{\mathbf{n}}_\sigma \,\mathrm{d}\mathscr{A}. \tag{3.3}$$

By using the conservation of potential density and the continuity equation [Eqs. (3.2) and (3.1)], the net, cross isopycnal flow can be related to the buoyancy forcing thus:

$$A(\sigma, t) = -\iint_{\mathscr{A}_\sigma(\sigma,t)} \nabla\cdot\mathbf{N}_\sigma\,|\nabla\sigma|^{-1}\,\mathrm{d}\mathscr{A} \tag{3.4}$$

showing that A is determined by the product of the buoyancy forcing $\nabla\cdot\mathbf{N}_\sigma$ and the isopycnal spacing (measured by $|\nabla\sigma|^{-1}$) integrated over the isopycnal surface. Thus

even if $\nabla\cdot\mathbf{N}_\sigma$ were spatially uniform, δA would not be zero if, as is typically the case, the isopycnal spacing is non-uniform.

Making use of the identity (a generalized form of Leibnitz theorem)

$$\frac{\partial}{\partial\sigma}\iiint_{R(\sigma,t)} a(\mathbf{x},t)\,\mathrm{d}V = \iint_{\mathscr{A}_\sigma(\sigma,t)} a(\mathbf{x},t)|\nabla\sigma|^{-1}\,\mathrm{d}\mathscr{A}$$

for any $a(\mathbf{x}, t)$, Eq. (3.4) can be written,

$$A(\sigma,t) = \frac{\partial B(\sigma,t)}{\partial\sigma} \tag{3.5}$$

where

$$B(\sigma,t) = -\iiint_{R(\sigma,t)} \nabla\cdot\mathbf{N}_\sigma\,\mathrm{d}V \tag{3.6}$$

is the *non-advective* supply of buoyancy to the volume R. Note that Eq. (3.5) is true at all times. The quantity $(-\partial B/\partial\sigma)\,\mathrm{d}\sigma$ is the non-advective buoyancy supply to the sub-region of R that has a density in the interval from σ-dσ to σ.

3.2. Estimating the net subduction from surface buoyancy fluxes

Formulae (2.6) and (3.5) tell us that the net subduction $\overline{M}$ can be calculated from a knowledge of the annual non-advective buoyancy-supply B given in Eq. (3.6). The integral in Eq. (3.6) can be converted to a surface integral by Gauss theorem. If R is chosen to extend below the entraining region of the mixed layer, then the dominant contributions to B are the buoyancy flux through the sea surface and diffusive fluxes across the bounding isopycnals.

Separating Eq. (3.5) into component parts, we may write it as, using the notation of Garrett et al. (1995):

$$\boxed{A = F - \frac{\partial D}{\partial\sigma}} \tag{3.7}$$

where F is the "transformation rate" defined by

$$F = \frac{\partial B_\mathrm{S}}{\partial\sigma} \tag{3.8}$$

and $\partial F/\partial\sigma$ can be called the "formation" because it gives the rate at which fluid is "squeezed" in to an isopycnal layer due to air–sea interaction.

Here

$$D = \iint_{\mathscr{A}_\sigma,\mathscr{A}_\mathrm{th}} \mathbf{N}_\sigma\cdot\mathbf{n}\,\mathrm{d}\mathscr{A} \tag{3.9}$$

is the non-advective (diffusive) flux across the surfaces $\mathscr{A}_\sigma$ and $\mathscr{A}_{\text{th}}$ and

$$B_S(\sigma, t) = -\iint_{\mathscr{A}_S(\sigma,t)} \mathscr{B}\, \mathrm{d}\mathscr{A} \tag{3.10}$$

can be calculated from a knowledge of the buoyancy flux $\mathscr{B}$ across the sea surface (dependent on fluxes of heat and fresh water).

Speer and Tziperman (1992) present monthly and annual averages of the function F in the North Atlantic. The contribution to the net subduction forced by the surface buoyancy-flux, which we will call $\overline{M}_S$, is

$$\overline{M}_S(\sigma) = \bar{F}(\sigma_1) - \bar{F}(\sigma).$$

As noted by Walin (1982), if the region $R(\sigma, t)$ is chosen so that the only open boundary is the sea surface, then $A = 0$ for a steady state and we have a balance between F and the convergence of diffusive fluxes across the bounding isopycnals of the volume. For example, this balance holds for the mean state of the world ocean if that mean state is not evolving. Of course, this is not the case here where we have an open boundary at the base of the winter mixed layer.

We now go on to discuss how $\overline{M}_S(\sigma)$ relates to $\overline{M}(\sigma)$ — are they very different and, if so, what is the mechanism and site of the diffusive fluxes that must occur to guarantee compliance with Eq. (3.7)? It is not possible to arrive at a definitive answer to these questions; moreover it is very difficult to make such inferences directly from data. We therefore make use of, through appropriate diagnosis, a numerical model of the ocean circulation. Although some of the details of our results will be dependent on model formulation, we believe that the broad conclusions we draw transcend the particular model we use and tell us useful things about the real ocean.

4. Diagnosis of transformation and subduction in a numerical model

The foregoing discussion is completely general, but to apply it in practice many approximations and assumptions have to be made. In addition one must confront the inadequacy, both in coverage and accuracy, of the relevant meteorological and oceanographic data sets. Despite these difficulties investigators have computed, individually, the "A" and "F" terms in Eq. (3.7). Marshall et al. (1993) studied the subduction field S, to which, through Eq (2.2) and (2.6), A is directly related. They diagnosed the currents using Levitus data employing thermal wind and, making use of linear vorticity balance to deduce the vertical velocity, deduced S from its kinematic definition (2.1). Speer and Tziperman (1992) computed F from climatological air–sea flux data sets. The errors in both calculations are undoubtedly significant but, on the whole, did not negate the conclusions drawn. However we are also interested in the pattern and mechanisms responsible for $\partial D/\partial\sigma$, which cannot be deduced directly from data. We have therefore chosen here to diagnose fields of A, F and $\partial D/\partial\sigma$ from a numerical model — the MIT model, Marshall et al. (1997a, b) — initialized with a hydrographic data set (again Levitus) and driven by analyzed fluxes from the

National Meteorological Center (NMC). This approach ensures that the individual terms are self-consistent and gives us insights into how the real ocean works.

4.1. The numerical integration

We make use of global integrations that were recently carried out at MIT for the purpose of model-data comparisons and to provide an initial estimate of the ocean circulation for state estimation. These efforts will be reported elsewhere — suffice it to say that the particular integration analyzed for transformation and subduction here is being closely scrutinized in the context of many different kinds of data — current meters, hydrography, surface elevation etc.

We now evaluate the various terms in Eq. (3.7) from the output of the model. The model, extending from 80°S to 80°N at 1° horizontal resolution, was configured with 20 levels in the vertical, ranging from 25 m at the surface to 500 m at the deepest level. Full spherical geometry and realistic topography was employed. The model was initialized with the "Levitus" data set and driven by 12-hourly winds and fluxes (obtained from the National Meteorological Center) during the period January 1983 until January 1996. A convective adjustment scheme (of the kind described in Klinger et al., 1996) was used to parameterize convection, and the wind stress was applied as a body force over the upper-most layer of the model. Note that the turbulent mixing induced by the wind is not represented in this model, hence the mixed layer is purely buoyancy driven.

The buoyancy flux is expressed in terms of heat and fresh water fluxes thus:

$$\mathscr{B} = \frac{g}{\rho_o}\left(\frac{\alpha}{c_w}\mathscr{H} + P_0\beta S(E-P)\right) \tag{4.1}$$

where c_w is the heat capacity of water, $\mathscr{H}$ is the surface heat loss, $E-P$ represents the net fresh water flux, α is the coefficient of thermal expansion of sea-water and β the haline contraction coefficient. In addition to the above fluxes the surface temperature was relaxed toward an evolving monthly averaged series of analyzed SST maps from NMC with a relaxation coefficient that was a function of space and time, as deduced by the climatological analysis of Barnier et al. (1995). The surface salinity was relaxed in the same way but to the monthly Levitus climatology.

The model exhibits much variability both on daily, seasonal and inter-annual time-scales. Of course, given the resolution of the model — 1° horizontally — baroclinic eddy transfers are not resolved and so must be parameterized.

We have set

$$\mathbf{N}_{\binom{T}{S}} = -\left[K_h \nabla_h \binom{T}{S} + K_v \frac{\partial}{\partial z}\binom{T}{S}\mathbf{k}\right] \tag{4.2}$$

where $\mathbf{k}$ is a unit vertical vector with K_h and K_v horizontal and vertical diffusivities, T is the (potential) temperature, and S is the salinity. In the numerical integration, K_v and K_h were set to constant values, $3\times10^{-5}\,m^2\,s^{-1}$ and $1000\,m^2\,s^{-1}$, respectively. We imagine that K_h crudely represents horizontal transfer due to baroclinic eddies and K_v vertical mixing due to internal waves.

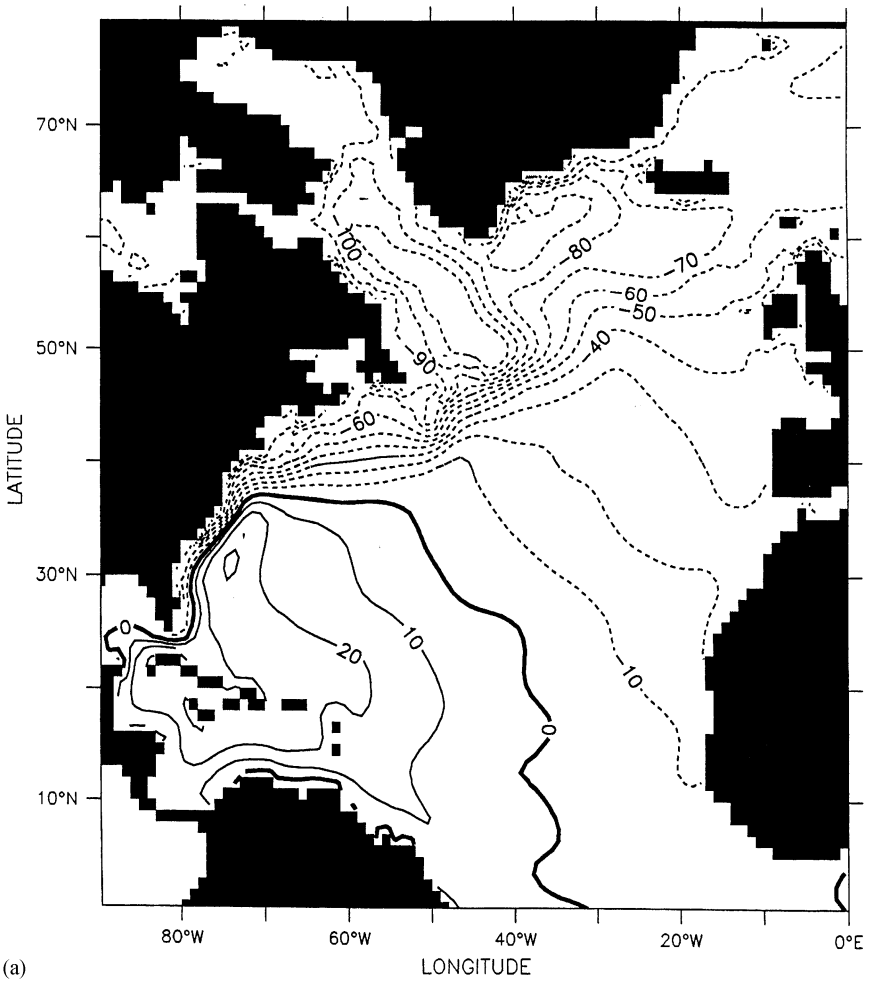

Fig. 4. (a) Model surface pressure field in March 92 (in cm, contour interval: 10 cm). (b) Outcrops in March 92 (contour interval: 0.2 kg m^{-3}).

The resulting circulation is plausible and exhibits many realistic features. Fields (3D velocity, pressure, temperature and salinity, air–sea fluxes, convection frequencies) were averaged monthly and diagnostics carried out on these monthly averaged fields.

Fig. 4a, the surface pressure field, reveals the broad sweep of the subtropical and sub-polar gyres. Fig. 4b shows the outcrops in March 1992. There is a broad range of σ values, from 20 at the equator off Africa to 27.8 in the Norwegian Sea. Note that north of roughly 30°N, outcrops have densities greater than 26. Hence, most of the horizontal density variations occur at low and middle latitudes. The mixed layer

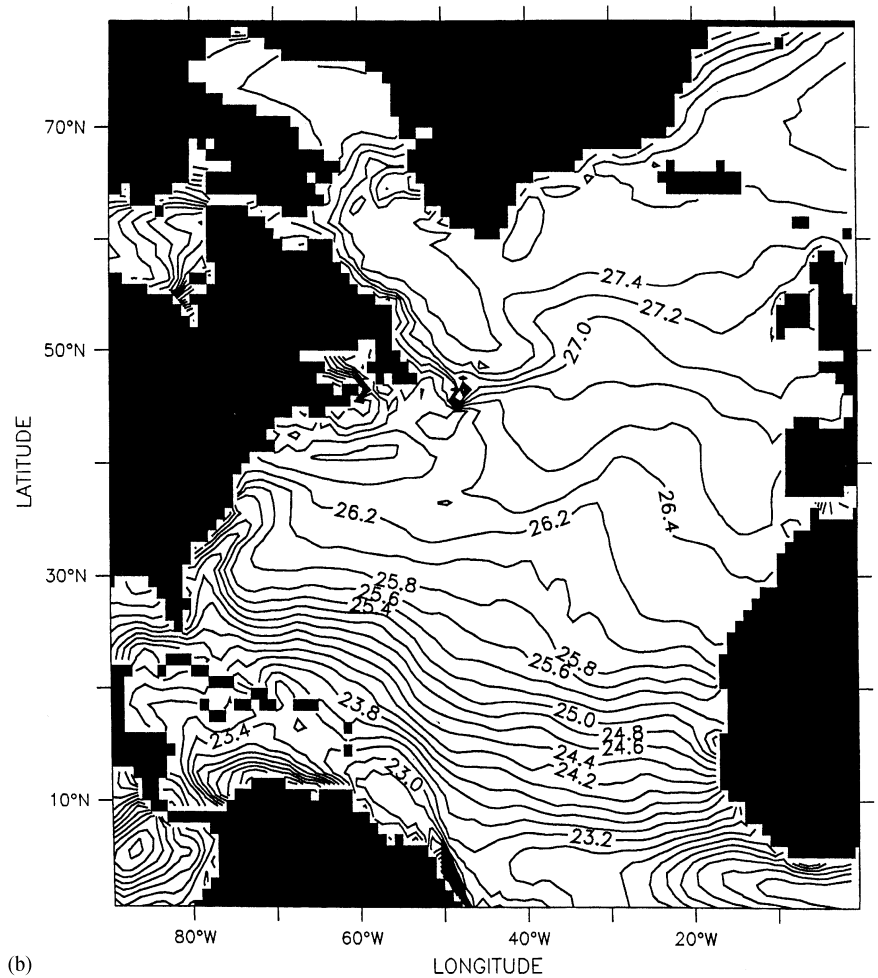

Fig. 4. (*continued*).

depth is diagnosed from the convection frequency index and is defined as the depth of the layer at which the convection frequency arrives at 0, starting from the surface. This definition guarantees that the mixed layer is always at least one model layer deep and is below the entraining region. The maximum of this field over the months of 1992 defines our control surface and looks very similar to the March mixed layer depth estimates (Fig. 5). The general pattern of $H(x, y)$ is familiar with a tongue of somewhat deeper — 200 m thick — layers extending southwestward across the basin. The mixed layer is particularly deep in the Labrador Sea, where it exceeds 2 km. In fact, the winter of 1991–92 was characterized by huge buoyancy losses over the Labrador Sea, and deep-water was found at a depth of 2500 m.

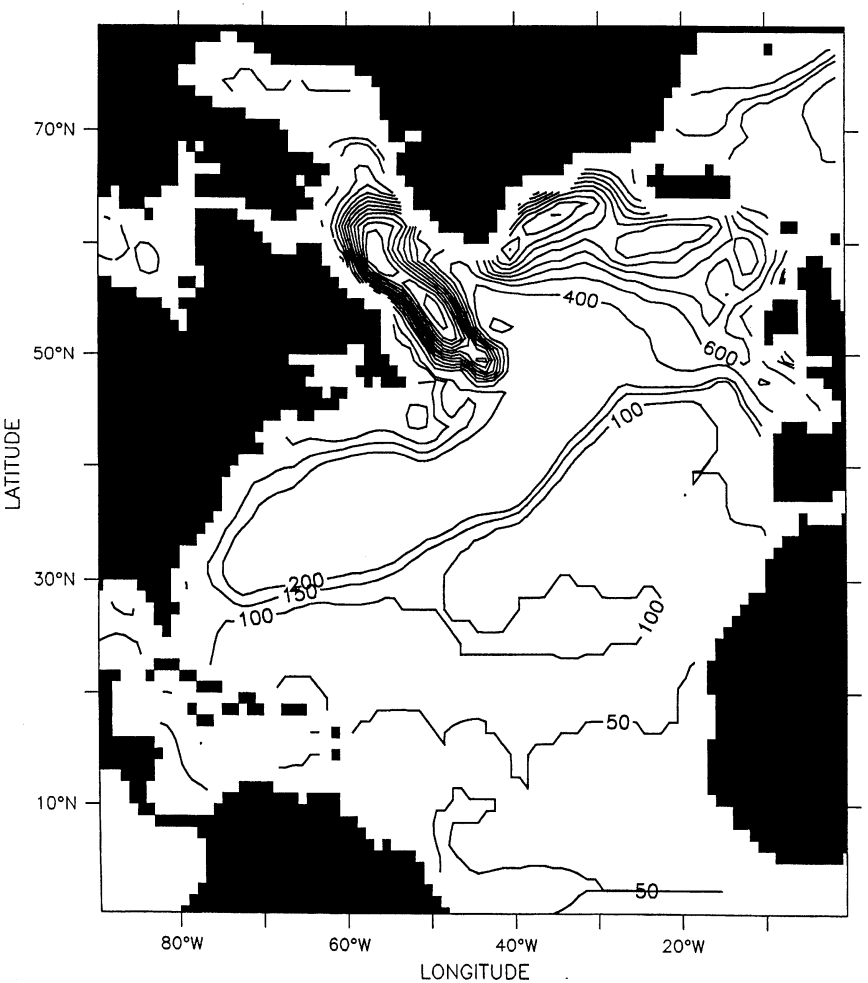

Fig. 5. Deepest mixed layer depth during 1992 (in m, contour interval: 50 m between 50 and 200 m, 200 m beyond). A three point boxcar window smoother has been applied along each axis.

4.2. *Computation of terms in* $A = F - \partial D/\partial\sigma$

We now consider the buoyancy budget over the North Atlantic basin, limited by the equator to the south, and extending all the way to 80°N (the northern boundary of the model). The Nordic Seas are included in the domain but not the Mediterranean Sea. Eq. (3.7) is valid at all times, but here we evaluate the different terms for each month of 1992 and then average over the year. A density bin $\delta\sigma$ of 0.2 is used. The details of the computation of the different terms are described in appendix A, together with an estimate of the discretization errors.

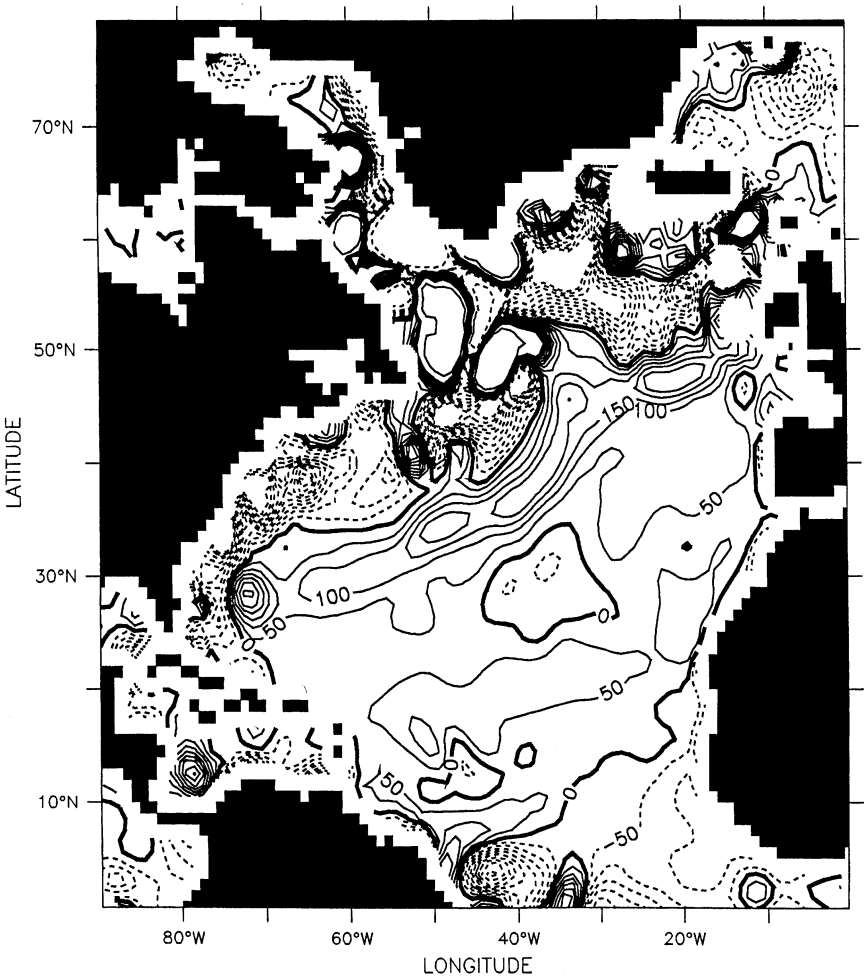

Fig. 6. Subduction rate in March 92 diagnosed from the model (in meters per year, contour interval: 50 m/yr between -500 and $+500$ m/yr, the isolines of -1000 and $+1000$ m/yr are also shown). A three points boxcar window smoother has been applied along each axis.

We will estimate the relative contributions of diapycnal volume flux, air–sea transformation and diffusion. Our interest is in the volume of fluid δR between $\sigma - \delta\sigma$ and σ, bounded by the sea surface at the top and the base of the winter mixed layer at the bottom (H field, see Fig. 5). Note that because of this choice, density values at the faces of the volume are not everywhere constant.

4.2.1. Subduction and diapycnal volume flux

The field of S is shown in Fig. 6. The large-scale distribution carries the imprint of the pattern of Ekman pumping/suction, the zero line roughly matching the zero

wind-stress curl line (not shown). However, due to the lateral induction term, the subduction field is enhanced wherever the mixed-layer depth has strong horizontal gradients: a zone of high subduction rates of the order of 100–200 m/yr extends across the basin from approximately 70°W, 30°N to 20°W, 50°N. This band corresponds to the main area of formation of subtropical mode waters, the density of which ranges roughly from 26 to 27 in the North Atlantic (see Fig. 4b). High entrainment rates are found north of this band with values greater than 500–1000 m/yr in many places. In the Labrador Sea, the distribution has smaller-scale features of high subduction and entrainment values. The broad pattern and magnitudes of S are qualitatively similar to those found by Marshall et al. (1993) deduced from Levitus data and the Isemer and Hasse climatology. However, the Marshall et al., estimate is much smoother due in part to the use of a smoother mixed-layer depth field.

Because the "S" field is rather noisy, the Eulerian fluid velocity contribution to A, which we call A_E, is computed directly (see Eq. (3.3)) by summing the volume fluxes along the boundary separating the region with densities greater than σ from the one with densities smaller than σ. Moreover, because the model exhibits variability on interannual time scales, we calculate explicitly the contribution A_v due to the movements of isopycnal surfaces (although this contribution is small when averaged over a year). Because the base of our control volume is fixed in time, at any instant there is a balance between the rate of change of V and A_v in Eq. (2.4). Note that A_v does not contribute to the integrated subduction M but has to be included when checking the balance (3.7) and inferring M from thermodynamics. A_v is estimated from $\partial V/\partial t$ in Eq. (2.4), calculated at each month using a centered-difference scheme and monthly estimates of the volume of the region δR. An integration backwards in density space yields A_v. The total diapycnal volume flux is obtained according to Eq. (3.3), and the average over the year 1992 is plotted in Fig. 7 along with its components.

Fig. 7 reveals a systematic pattern: A is slightly negative in the tropics in the density range $20 \rightarrow 23$ (see Fig. 4b) but is directed northward outside the tropics towards higher densities. It is interesting that A systematically increases from $\sigma = 23$ (at roughly 10°N in March on the southern flank of the subtropical gyre) all the way up to $\sigma = 25.6$ (at roughly 25°N in March) reaching 13 Sv at $\sigma = 25.6$. This implies a net flux of mass *from* the interior *to* the mixed-layer in these density ranges, integrated across the basin, despite the fact that in the interior of the gyre, at least, Ekman pumping is directed downward over this latitude range. Note, however, that A represents a diapycnal volume flux integrated along the out-cropping isopycnal from one coast to the other. Because the outcrops are orientated from SE to NW, and the S field is orientated from NE to SW (reflecting the tilt of the zero wind-curl line) there is much cancellation. For example in the subtropical gyre water floods down into the ocean from the outcrop window in the interior, but much of it returns to the surface layer as the western boundary current flows northward again.

As expected, A_v is small when averaged over a year, reaching an amplitude of at most 2–3 Sv (at $\sigma = 23.2$ and $\sigma = 27.4$). The Eulerian fluid component A_E has been further separated into a geostrophic contribution A_{Eg} and a reminder A_{Eag}, which includes all the ageostrophic contributions (Ekman drift, vertical flow, …). A_{Eg} is positive over the entire domain and not negligible, particularly in high density ranges

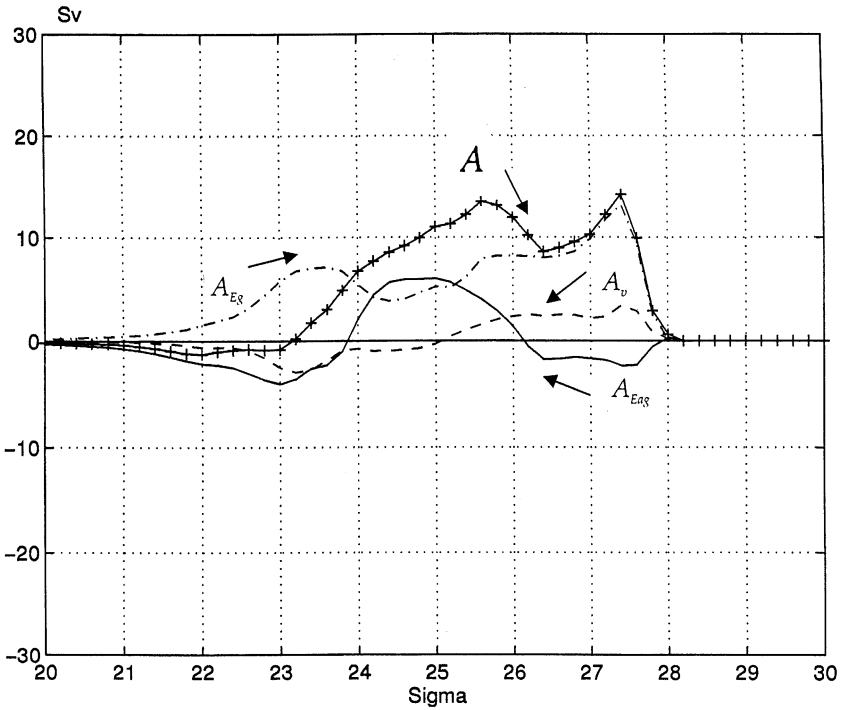

Fig. 7. Annual diapycnal volume flux A and its components (in Sv) between the sea surface and the base of the winter mixed layer for the year 1992. Solid line with " + ": total A; dashed-dot line: geostrophic component A_{Eg}; dashed line: volume change component A_v; solid line: ageostrophic component A_{Eag}.

($\sigma > 26$). Note that in this density range, A_{Eag} is negative and thus points to the south. For $\sigma < 26$, A_{Eag} and A_{Eg} are of comparable magnitude. Hence the geostrophic contribution is found to be very important and certainly not small relative to the Ekman drift as was hypothesized by Tandon and Garrett (1997). In particular, the export of water towards higher densities for $\sigma > 26$ is achieved largely by the geostrophic currents.

4.2.2. Air–sea transformation

The transformation F is evaluated using Eqs. (3.8) and (3.10) (see appendix for details) and is shown in Fig. 8. In the class range (20–24), F shows negative values with a minimum of about -24 Sv at $\sigma = 22.8$. Air–sea flux tends to create lighter water in this density range. For densities greater than 24, F is positive with two maxima: one of 20 Sv at $\sigma = 26$, and the other of 22 Sv at $\sigma = 27.6$. In this density range, F tends to transform water from lighter class to denser class. Note that A and F are indeed of different sign in the $23 \rightarrow 24$ range, as noted by Tandon and Garrett (1997) reviewing inferences made from data.

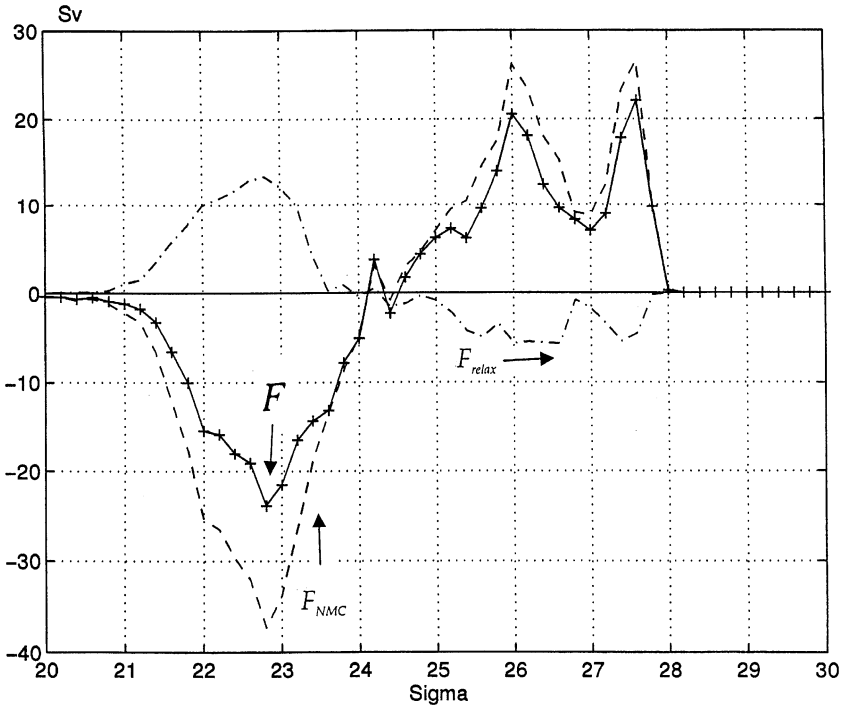

Fig. 8. Annual air–sea transformation rate F and its components (in Sv) for the year 1992. Solid line with " + ": total F; dashed line: NMC component F_{NMC}; dashed-dot line: restoring terms component F_{relax}.

Of the two components that make up F, the contribution from the NMC fluxes, F_{NMC}, is the most important, but the relaxation term is also significant. Qualitatively, the general structure of F is very similar to that found by Speer and Tziperman (1992) using the Isemer and Hasse data set. With a density bin of 0.1, their estimate shows a minimum of -7.6 Sv at $\sigma = 23$ and a maximum of 32.2 Sv at $\sigma = 26.1$. A maximum for higher density values is absent, but their data set extends to 65°N only, excluding the Nordic Seas. Furthermore, their estimate is inferred from a climatological data set, whereas the present one comes from an annual average.

It is interesting to note that A and F have a similar qualitative form for densities greater than 24 (compare Figs. 7 and 8). They both have the same sign and show two maxima in roughly the same density ranges. In fact, as noted in Section 3, A and F would be identical if there were no mixing. Note also that the slopes of A and F have generally the same sign. However, the water mass formation rates implied by air–sea fluxes are higher. For example, in the range $26 \rightarrow 27$, which spans the densities of subtropical mode waters, there is a creation of 12 Sv by air–sea fluxes whereas the integrated subduction is only 2 Sv in this density range (see Fig. 7). Inspection of the difference $F-A$ shows that there is indeed significant transformation by mixing (Fig. 9), particularly in density ranges lighter than 24. In the class (21–25.6), A is

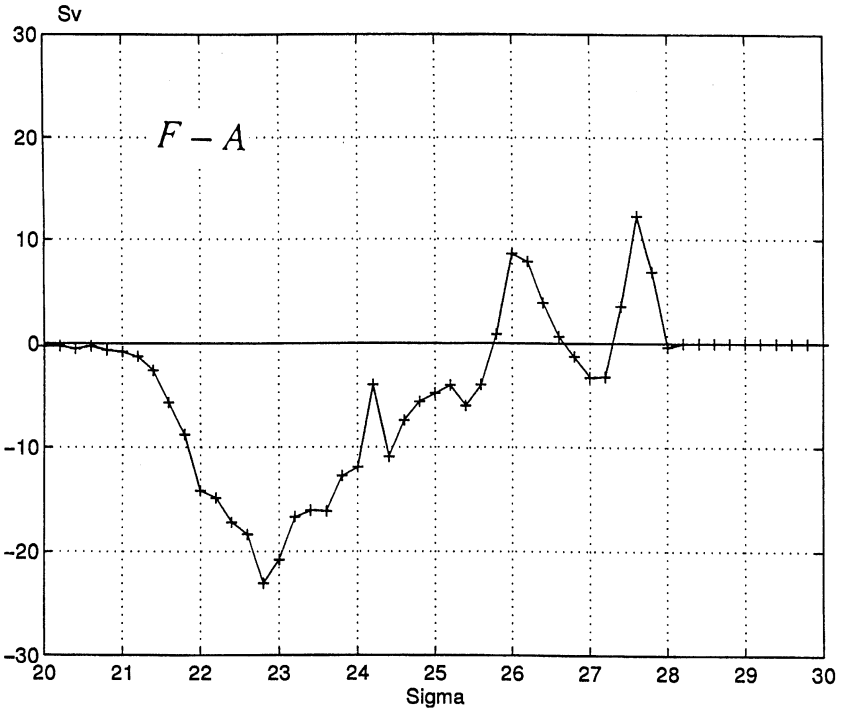

Fig. 9. Annual difference F–A (in Sv) for the year 1992.

greater than F (they differ by 22 Sv at $\sigma = 22.8$). The diapycnal advective flux is not able to carry away all the buoyancy supplied by air–sea fluxes. Hence, some mixing processes must accommodate this excess buoyancy and redistribute it. For densities greater than $\sigma = 25.8$, the situation is reversed: F is now greater than A over most of these density ranges (mismatch of about 12 Sv at $\sigma = 27.6$), and mixing must supply buoyancy to help balance the substantial buoyancy loss to the atmosphere. In order to identify the origin and location of the mixing, we now turn to the computation of diffusive fluxes.

4.2.3. Diffusive fluxes

In the region "δR", the diffusive contributions to the buoyancy budget arise from (i) the diapycnal diffusive fluxes across the isopycnals $\sigma - \delta\sigma$ and σ, and (ii) the diffusive flux across the winter mixed layer base [see Eq. (3.9)]. Thus we separate $(\partial D/\partial\sigma)$ in to a diapycnal term, $(\partial D_{\mathrm{dia}}/\partial\sigma)$, which accounts for the *difference* between the diapycnal diffusive flux across the isopycnal σ, and that across the isopycnal $\sigma - \delta\sigma$, and a contribution, $(\partial D_{\mathrm{mld}}/\partial\sigma)$, which represents the diffusive flux across the surface defined by the base of the winter mixed layer, integrated along the window $(\sigma - \delta\sigma, \sigma)$. This latter flux makes a non-negligible contribution because, particularly

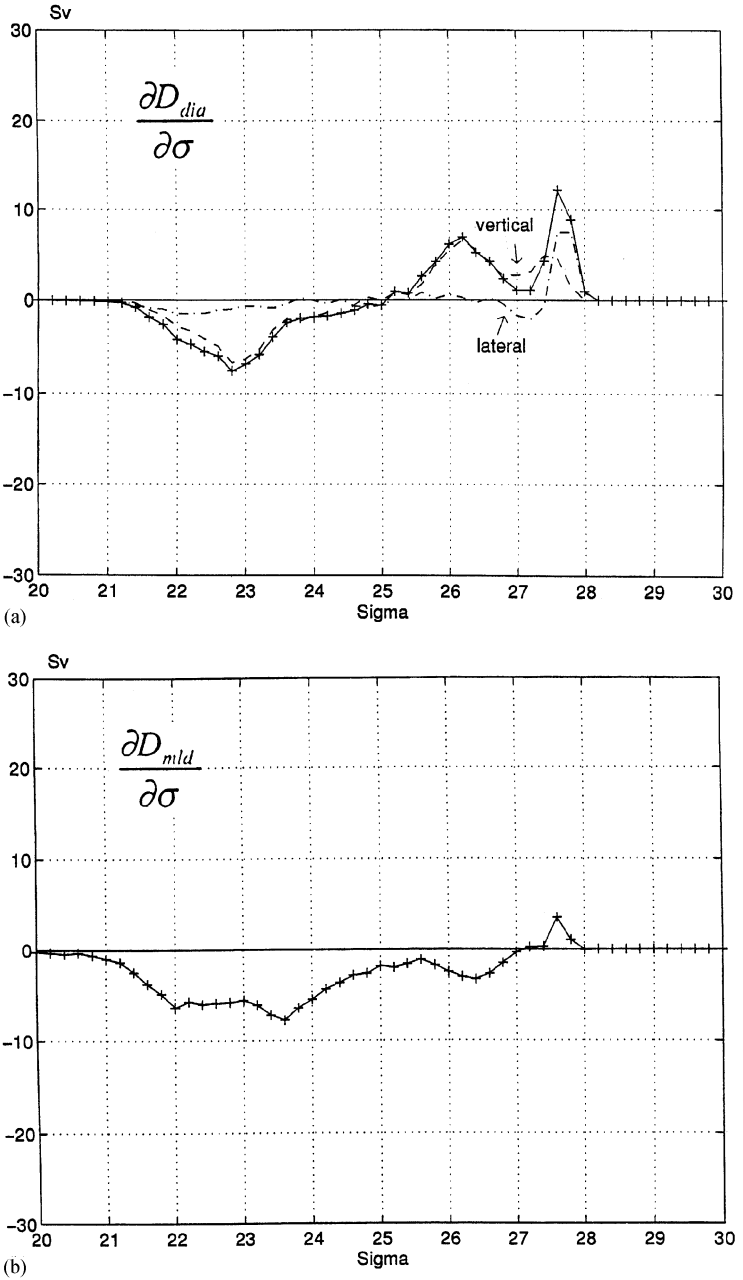

Fig. 10. (a) Annual transformation due to the convergence of diapycnal diffusive buoyancy fluxes between the sea surface and the base of the winter mixed layer for the year 1992. Solid line with " + ": total $\partial D_{\mathrm{dia}}/\partial\sigma$; dashed line: vertical component; dashed-dot line: lateral component. (b) Annual transformation due to diffusive buoyancy fluxes across the base of the winter mixed layer for the year 1992.

in the tropics where the thermocline is shallow and strong, there is stratification at the base of the mixed layer and the latter is nearly parallel to isopycnals there.

4.3. Diapycnal fluxes

The convergence of diapycnal diffusive fluxes is shown in Fig. 10a. Diapycnal mixing acts to remove buoyancy in the class range (21–25), whereas the opposite is observed for densities greater than 25, which is expected from the F–A pattern (Fig. 9). In particular, the diapycnal diffusive flux convergence seems to account for most of the mismatch between A and F at high latitudes. The mixing is not sufficient in the tropics, however. Overall, the diapycnal diffusive flux convergence tends to counteract the effect of air–sea flux (it removes buoyancy in areas where there is supply from F and vice versa). Indeed, $(\partial D_{\mathrm{dia}}/\partial\sigma)$ appears as an attenuated mirror image of F, which is not surprising in view of the tendency of $(\partial D_{\mathrm{dia}}/\partial\sigma)$ to balance F in a closed volume over a year.

The diapycnal mixing can be separated into a lateral and vertical component. The lateral contribution is significant at high latitudes, where a transformation of about 8 Sv is diagnosed at 27.6 and 27.8. Of these 8 Sv, 50% occurs in the mixed layer in winter (not shown). The other half occurs in the seasonal thermocline during summer, when a bolus of unstratified water of densities of 27.6 and 27.8 lies in the interior below the stratified upper layer (not shown). The restratification process, which in nature is probably associated with baroclinic eddy transfer processes, is not well represented in the model. For all other density ranges, the transformation induced by vertical mixing dominates and occurs in the seasonal thermocline. In the class (22– 24), the isopycnals are shallow and subject to mixing across the base of the mixed layer where the stratification is strong. Vertical mixing acts to remove buoyancy out of the control volume in this density range. For densities greater than 25, the winter mixed layer can be substantially deeper than the summer mixed layer (see Figs. 4b and 5), and vertical mixing acts to supply buoyancy in the control volume there.

4.4. Flux across the winter mixed layer base

There is a diffusive contribution $(\partial D_{\mathrm{mld}}/\partial\sigma)$ to the buoyancy budget of the region δR across the surface defined by the winter mixed layer base. As expected, this latter term is significant for low density ranges $21.5 \rightarrow 24.5$, negative over most of the domain, in the sense to remove buoyancy from the control volume. There is a slight contribution from lateral fluxes (due to the slope of the winter mixed layer base) that is responsible for the small buoyancy gain at high latitudes ($+3$ Sv at 27.6). It is interesting to note that in the density range (22–24), the two diffusive contributions both act to remove buoyancy out of the control volume and have comparable order of magnitude (see Fig. 10a and b). Together, they remove about 10 Sv in the class 22–24, the class for which the transformation by mixing is the most important.

Finally in Fig. 11 we plot the residual $F - A - (\partial D/\partial\sigma)$. Typically, the residual is less than 5 Sv except at lower density ranges (where it reaches -10 Sv at $\sigma = 22.8$). Overall, though, the residual is significantly smaller than the difference F–A; the rms

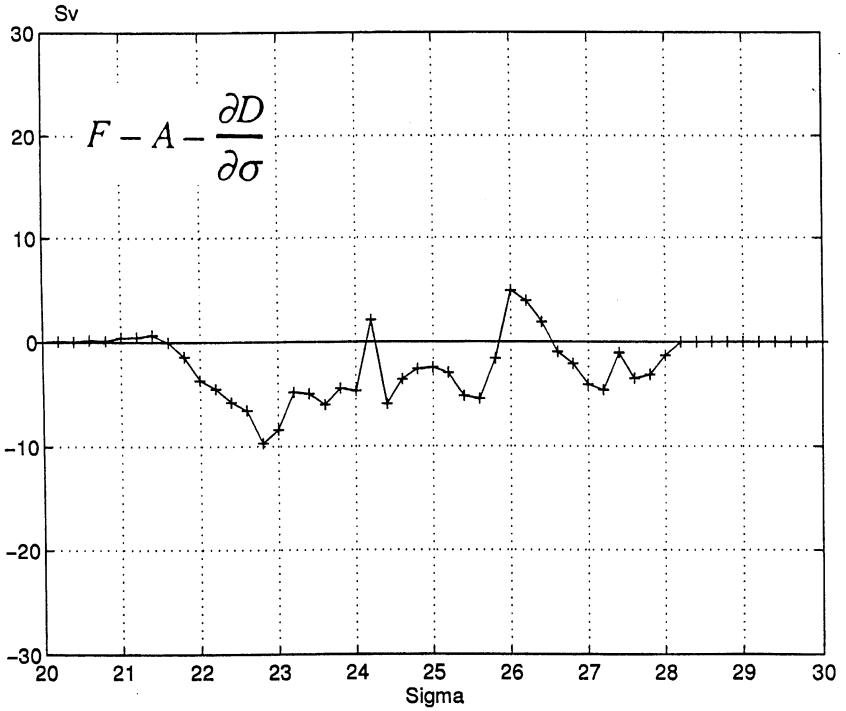

Fig. 11. Annual residuals of the balance $A = F - \partial D/\partial\sigma$ for 1992.

of the residual is 3 Sv, compared to 8 Sv for F–A. The origin of these residuals, a consequence of the isentropic analysis being carried out in the context of a non-isentropic numerical model, is discussed in detail in Appendix B.

5. Discussion and conclusions

5.1. Our main conclusions are as follows:

1. Imposed gradients of buoyancy forcing at the sea surface, B_s, (loss at high latitudes, gain at low latitudes) induce transformation of water from light to dense, and a formation of water of denser classes ($F > 0$, poleward of $\sigma = 23$) and a destruction of water in lighter density classes ($F < 0$, equatorward of $\sigma = 23$), as sketched schematically in Fig. 12.
2. Diffusive transfer of buoyancy within the mixed layer and seasonal thermocline opposes these tendencies and attenuates the influence of F. The dominant part of this contribution comes from vertical mixing. In high latitudes, lateral fluxes provide an additional significant transfer of buoyancy.

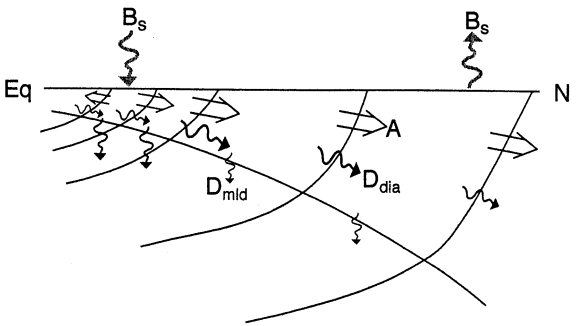

Fig. 12. Schematic diagram showing the balance and sense of the buoyancy budget of the upper boundary layer of the ocean.

3. The net effect is a predominantly poleward diapycnal volume flux A. For densities greater than 26, this poleward flux is achieved largely by the geostrophic component. In certain density classes A and F are of opposite sign and can differ by as much as 20 Sv.
4. The pattern of A is consistent with, and can be understood as a consequence of, the integrated affect of interior and widespread subduction of fluid over the subtropical gyre, and localized and intense entrainment on the western margin, summed over the outcrop window from coast to coast.
5. Overall, F is not a good predicator of A. Mixing is significant everywhere in the upper boundary layer of the ocean model and must be invoked to reconcile the kinematic and thermodynamic methods.

Does the model diagnosed here assume that levels of mixing are unrealistically large? The importance of vertical mixing in the tropics is consistent with earlier studies. For example, Walin (1982) noted that due to the tendency of light water to spread over heavier water, the diapycnal volume flux must be poleward in all density ranges. Hence mixing is essential in regions where the air–sea fluxes transform water towards lighter densities. The diagnostic studies of McWilliams et al. (1996) and Nurser et al. (1998) have further suggested that mixing in the tropics could be related to the upwelling occurring on the eastern side of the basin off Africa inducing strong vertical gradients. Here, the mixing across the base of the mixed layer is accomplished through vertical diffusive fluxes with $K_v \approx 3 \times 10^{-5}\,m^2/s$, not an unreasonably high value and roughly in accord with estimates of Speer (1997) inferred from data. The lateral diffusive fluxes across the vertically inclined isopycnals of the mixed layer and seasonal thermocline require further work but are likely to be associated with baroclinic instability. For example the study of Haine and Marshall (1998) shows that eddy-diffusivities of $1000\,m^2/s$ (as assumed in the model study here) can readily be achieved by baroclinic instability processes in deep (in excess of a few 100 m) mixed layers. Thus we believe that our model is not so diffusive as to render it inappropriate

to its application here. The role of the restratification process at high latitudes in spring and summer needs better representation, however.

In summary, then, we have seen that we are able to reconcile kinematic and thermodynamic methods by invoking plausible levels of mixing in the framework of a numerical model, and believe that our results provide guidance for interpreting ocean data. In the future, models including an active mixed layer and more realistic parameterizations of baroclinic eddy transfers should help clarify and determine the relative roles of baroclinic instability, entrainment fluxes at the base of the mixed layer, and mixing in the interior.

Acknowledgements

This study was supported by the Physical Oceanography program of NSF. Comments from Amit Tandon, George Nurser, and an anonymous reviewer are greatly acknowledged.

Appendix A. numerical computation of F, A, and $\partial D/\partial\sigma$

In what follows, the expressions of F, A, and $\partial D/\partial\sigma$ are written for a given month t. The estimates shown in Figs. 7–11 are obtained by simply taking the arithmetic average of the monthly estimates (for 1992). Integer indices i, j, k refer to grid cells centered at tracer points on the staggered C-grid. We define a 1D grid of density points σ_n ($n = 1, \ldots, N$) of constant grid step $\delta\sigma$. The points at which "flux" quantities (volume and diffusive fluxes) are naturally evaluated are noted $\sigma_{n+1/2}$ ($= \sigma_n + \delta\sigma/2$). The sums below always run all over the model domain, and the boxcar functions Π are set to zero outside the North Atlantic basin.

A.1. Air–sea flux F

F is evaluated using Eqs. (3.8) and (3.10), namely,

$$F(\sigma_n, t) = \frac{\delta B(\sigma_n, t)}{\delta\sigma} = -\frac{1}{\delta\sigma}\sum_{ij} b(i,j,t) \times a(i,j) \times \Pi_{\mathrm{F}}(\sigma_n, \sigma(i,j,1,t)) \tag{A.1}$$

where $b(i,j,t)$ is the air–sea density flux (> 0 to the atmosphere) evaluated from the heat and freshwater fluxes at month t, $a(i,j)$ is the horizontal area at position (i,j), $\sigma(i,j,1,t)$ is the potential density referenced to the surface (evaluated from the temperature and salinity at month t, with the equation of state used in the model integration),

$$\Pi_F(\sigma_n, \sigma(i,j,1,t)) = \begin{cases} 1 & \text{if } \sigma_n - \delta\sigma/2 < \sigma(i,j,1,t) < \sigma_n + \delta\sigma/2 \\ 0 & \text{otherwise.} \end{cases}$$

Eq. (A.1) is used for both the total density flux and the NMC contribution. The contribution from the relaxation terms is inferred by subtraction.

A.2. Diapycnal volume flux

The Eulerian fluid component A_E is evaluated using Eq. (3.3):

$$\begin{aligned} A_E(\sigma_{n+1/2}, t) = & \\ & \sum_{ijk} \pm u\,(i-\tfrac{1}{2}, j, k, t) \times a_u(i-\tfrac{1}{2}, j, k) \times \Pi_u(\sigma_{n+1/2}, \sigma(i-1, j, k, t), \quad \sigma(i, j, k, t)) \\ & + \sum_{ijk} \pm v(i, j-\tfrac{1}{2}, k, t) \times a_v(i, j-\tfrac{1}{2}, k) \times \Pi_v(\sigma_{n+1/2}, \sigma(i, j-1, k, t), \sigma(i, j, k, t)) \\ & + \sum_{ijk} \pm w(i, j, k-\tfrac{1}{2}, t) \times a(i, j) \times \Pi_w(\sigma_{n+1/2}, \sigma(i, j, k-1, t), \sigma(i, j, k, t)) \end{aligned} \tag{A.2}$$

where the sign in front of each term is the sign of the component of $\nabla\sigma$ at that point (guaranteeing that the volume fluxes are > 0 towards higher densities) and:

u, v, w are the zonal, meridional, and vertical components of the velocity field, $a_u(i-1/2, j, k)$ is the area of the face common to grid cells (i, j, k) and $(i-1, j, k)$, $a_v(i, j-1/2, k)$ is the area of face common to grid cells (i, j, k) and $(i, j-1, k)$,

$$\Pi_u(\sigma_{n+1/2}, \sigma(i-1, j, k, t), \sigma(i, j, k, t)) = \begin{cases} 1 \text{ if } \begin{cases} \sigma(i-1, j, k, t) < \sigma_{n+1/2} < \sigma(i, j, k, t) \\ (\text{assuming } \sigma\ (i-1, j, k, t) < \sigma(i, j, k, t)) \\ \text{dpth}(k) > -H(i, j) \\ \text{dpth}(k) > -H(i-1, j) \end{cases} \\ 0 \text{ otherwise.} \end{cases}$$

dpth(k) is the depth (< 0) of tracer points at level k and $H(i, j)$ is the deepest mixed layer depth (> 0) at position (i, j) over the year 1992. Π_v and Π_w have similar expressions.

The geostrophic component A_{Eg} is computed by replacing u, v, w by u_g, v_g, 0 in (A.2) where u_g and v_g are the zonal and meridional geostrophic velocities respectively (computed from the pressure field). The ageostrophic component is inferred by subtraction.

The component A_v due to the movement of isopycnal surfaces balances the rate of change of the volume V in Eq. (2.4) (see Section 4.2). In discrete form:

$$\frac{\partial \delta V(\sigma_n, t)}{\partial t} = A_v(\sigma_{n-1/2}, t) - A_v(\sigma_{n+1/2}, t)$$

The time-derivative is evaluated using volume estimates at each month and a centered-difference scheme. For each month, the volume is estimated as follows:

$$\delta V(\sigma_n, t) = \sum_{ijk} \text{vol}(i, j, k) \times \Pi_{\text{vol}}(\sigma_n, \sigma(i, j, k, t)) \tag{A.3}$$

where vol(i, j, k) is the volume of grid cell (i, j, k),

$$\Pi_{\mathrm{vol}}(\sigma_n, \sigma(i,j,k,t)) = \begin{cases} 1 \text{ if} & \begin{cases} \sigma_n - \dfrac{\delta\sigma}{2} < \sigma(i,j,k,t) < \sigma_n + \dfrac{\delta\sigma}{2} \\ \mathrm{dpth}(k) > -H(i,j) \end{cases} \\ 0 \text{ otherwise.} \end{cases}$$

A_{v} is then evaluated at $\sigma_{n+1/2}$ points by integrating backwards in density space and setting $A_{\mathrm{v}}(\sigma = \sigma_{N+1/2}) = 0$. The total diapycnal volume flux $A(= A_{\mathrm{E}} + A_{\mathrm{v}})$ is finally interpolated linearly at σ_n points.

A.3. Diffusive fluxes

The computation of the diffusive fluxes is done in two steps. First, δD is evaluated using Eq. (3.6):

$$\delta D(\sigma_n, t) = \sum_{ijk} \nabla\cdot \mathbf{N}_\sigma(i,j,k,t) \times \mathrm{vol}(i,j,k) \times \Pi_{\mathrm{vol}}(\sigma_n, \sigma(i,j,k,t)) \tag{A.4}$$

where the boxcar function is the same as the one used just above and where:

$$\mathbf{N}_\sigma = \boldsymbol{K}\nabla\sigma \quad \text{with } \boldsymbol{K} = \begin{pmatrix} K_{\mathrm{h}} & 0 & 0 \\ 0 & K_{\mathrm{h}} & 0 \\ 0 & 0 & K_{\mathrm{v}} \end{pmatrix}$$

K_{h} and K_{v} are horizontal and vertical constant diffusivities coefficients, respectively. The divergence is evaluated as in the model integration [see Eq. (21) in Marshall et al., 1997b].

The diapycnal contribution to δD is then evaluated from the total diapycnal diffusive flux D_{dia} at points $\sigma_{n+1/2}$. This flux is computed in the same way as the diapycnal volume flux ($\pm\, u(i-\frac{1}{2}, j, k, t)$ replaced by $-K_{\mathrm{h}} \times |(\partial\sigma/\partial x)(i-\frac{1}{2}, j, k, t)|$ in Eq. (A.2) and similar changes for v and w components). The flux convergence is then evaluated simply according to:

$$\frac{\delta D_{\mathrm{dia}}}{\delta\sigma}(\sigma_n, t) = \frac{D_{\mathrm{dia}}(\sigma_{n+1/2}, t) - D_{\mathrm{dia}}(\sigma_{n-1/2}, t)}{\delta\sigma}$$

The contribution from diffusive fluxes in the "instantaneous" mixed layer is evaluated similarly except that $H(i,j)$ is replaced by $h(i,j,t)$ — mixed layer depth at month t ($H(i,j) = \max_t[h(i,j,t)]$) — in the definition of the boxcar function Π_{u}.

The diffusive contribution across the base of the winter mixed-layer δD_{mld} is obtained by subtraction:

$$\frac{\delta D_{\mathrm{mld}}}{\delta\sigma}(\sigma_n, t) = \frac{\delta D}{\delta\sigma}(\sigma_n, t) - \frac{\delta D_{\mathrm{dia}}}{\delta\sigma}(\sigma_n, t).$$

Appendix B. Error analysis

There are two sources of error responsible for the residuals on Fig. 11. One is a discretization error related to the use of height coordinate for budgets in isopycnal layers, the other is due to residuals in the buoyancy equation (3.2), integrated over the volume $\delta R(\sigma, t)$.

B.1. Discretization error

The relation (3.7) $A = F - \partial D/\partial\sigma$ is derived under the assumption that density values along the faces of the region $\delta R(\sigma, t)$ are constant. This is not the case in the discrete model in which temperature and salinity values are interpolated onto the faces. The resulting error $e1(\sigma, t)$ (expressed as a volume flux) can be written:

$$e1(\sigma, t) = \frac{1}{\delta\sigma} \iint_{\mathscr{A}_\sigma, \delta\mathscr{A}_{\text{th}}} \Delta\sigma \mathbf{v}\cdot\mathbf{n}\, \mathrm{d}\mathscr{A} \tag{B.1}$$

where $\Delta\sigma$ is the difference between the interpolated density value and the constant one. The double integral is over the faces of the region $\delta R(\sigma, t)$. The annual average of $e1(\sigma, t)$, is shown in Fig. 13. The values are less than ± 5 Sv for the most part, with a minimum of -6 Sv at $\sigma = 22.8$ accounting for 60% of the residual of Fig. 11 for this density.

In the tropics, there is a systematic error at the base of the control surface because the latter is nearly parallel to isopycnals there. The density difference, $\Delta\sigma_{\text{mld}}$, can be expressed as $\Delta\sigma_{\text{mld}} \sim (\partial\sigma/\partial z)_{\text{mld}} \times \Delta z$ where $(\partial\sigma/\partial z)_{\text{mld}}$ is the stratification at the base of the mixed layer and Δz the vertical resolution of the model. Using $(\partial\sigma/\partial z)_{\text{mld}} \sim 40\ \text{kg m}^{-3}/\text{km}$ and $\Delta z \sim 25$ m, we find that $\Delta\sigma_{\text{mld}} \sim 1\ \text{kg m}^{-3}$ or five times the density bin $\delta\sigma$ used here. The relation (3.7) does not apply well there in the sense that the density values at the base of the control volume are — using the notation of appendix 1 — greater than $\sigma_n + \delta\sigma/2$. Hence, the density values at the base of the control volume implied by relation (3.7) are underestimated in the tropics, giving rise to the residuals observed in Fig. 13a. The only way to reduce this error would be to increase the model vertical resolution. A similar problem also occurs on the horizontal but the density difference $\Delta\sigma$ is of the order of the density bin at most and not always of the same sign. However, its contribution to (A.3) can be significant when integrated along the deep winter mixed layers at high latitudes (see Fig. 13a).

B.2. Residuals in the buoyancy equation

These residuals, expressed in Sv and averaged over a year, are shown in Fig. 13b. They are negative everywhere and less than 5 Sv for the most part. They arise from terms that have not been taken into account in the buoyancy equation and from errors due to the use of monthly averaged fields as opposed to instantaneous fields. These residuals could be reduced to zero if all the terms of Eq. (3.2) were dumped and

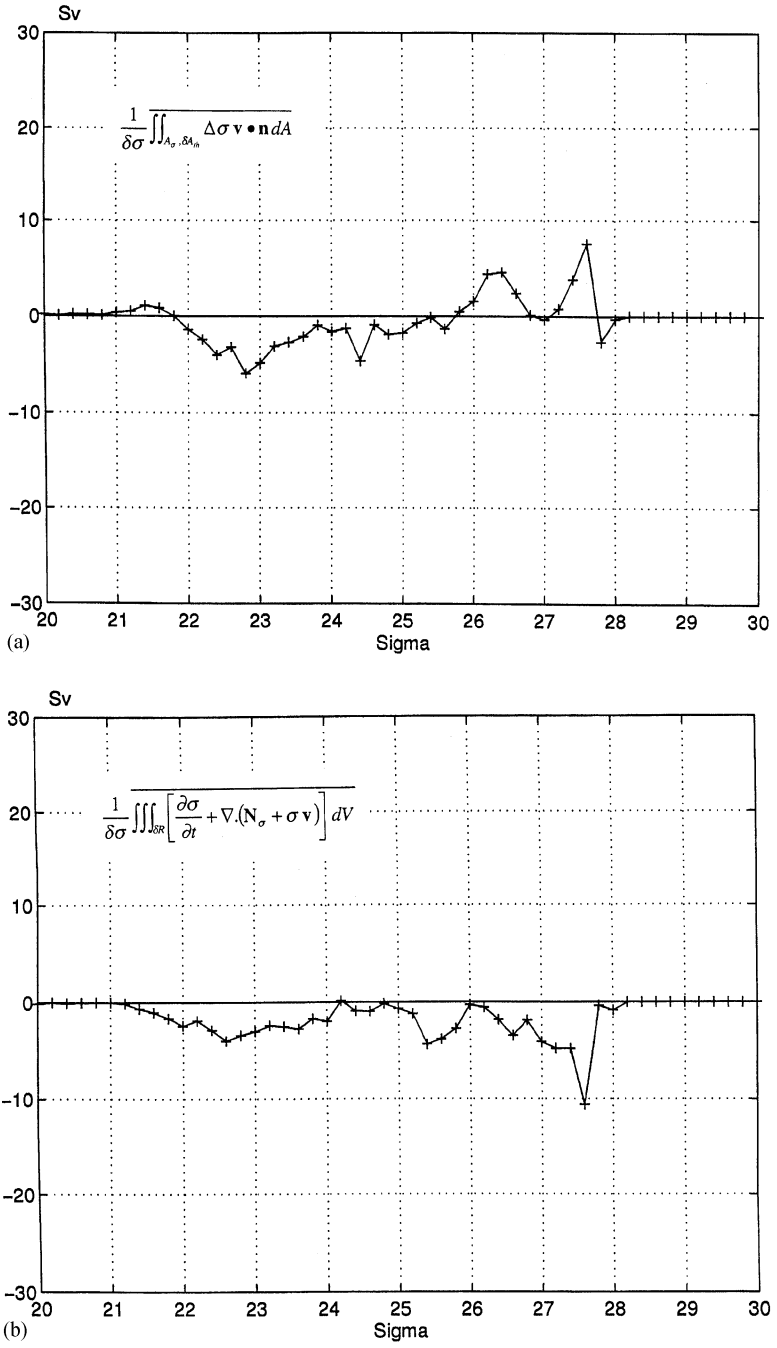

Fig. 13. (a) Discretization error (in Sv) for the year 1992. (b) Annual residuals (in Sv) of buoyancy equation integrated over region $\delta R(\sigma, t)$ for the year 1992.

averaged in the same way. Even in this case, though, the discretization error would remain.

Interestingly, the residuals in Fig. 11 appear to be simply the sum of Figs. 13a and b and can be interpreted in the following way: they are the average, over a year, of the residuals of the buoyancy equation integrated over the volume $\delta R(\sigma, t)$ at each month, where the advective buoyancy flux convergence $\iint_{\mathscr{A}_\sigma, \delta\mathscr{A}_{\rm th}} \sigma \mathbf{v} \cdot \mathbf{n}\, \mathrm{d}\mathscr{A}$ is computed assuming that the density values are constant at the faces of the volume.

References

Barnier, B., Siefridt, L., Marchesiello, P., 1995. Thermal forcing for a global ocean circulation model using a 3 yr climatology of ECMWF analyses. Journal of Marine Systems 6, 363–380.

Garrett, C., Speer, K., Tragou, E., 1995. The relationship between water mass formation and circulation, with application to Phillips' Red Sea model. Journal of Physical Oceanography 25, 1696–1705.

Garrett, C., Tandon A., 1997. The effects on water mass formation of surface and mixed layer time-dependence and entrainment fluxes. Deep-Sea Research I 44, 1991–2006.

Haine, T.W.N., Marshall, J.C., 1998. Gravitational, symmetric and baroclinic instability of the ocean mixed layer. Journal of Physical Oceanography 28, 634–658.

Huang, R.X., Qiu, B., 1994. Three-dimensional structure of the wind-driven circulation in the subtropical North Pacific. Journal of Physical Oceanography 24, 1608–1622.

Klinger, B., Marshall, J., Send, U., 1996. Representation of convective plumes by vertical adjustment. Journal of Geophysical Research 101, 18175–18182.

Marshall, J.C., Nurser, A.J.G., 1992. Fluid dynamics of oceanic thermocline ventilation. Journal of Physical Oceanography 22, 583–595.

Marshall, J.C., Nurser, A.J.G., Williams, R.G., 1993. Inferring the subduction rate and period over the North Atlantic. Journal of Physical Oceanography 23, 1315–1329.

Marshall, J.C., Hill, C., Perelman, L., Adcroft, A., 1997a. Hydrostatic, quasi-hydrostatic, and nonhydrostatic ocean modeling. Journal of Geophysical Research 102, 5733–5752.

Marshall, J.C., Adcroft, A., Hill, C., Perelman, L., Heisey, C., 1997b. A finite volume, incompressible Navier Stokes model for studies of the ocean on parallel computers. Journal of Geophysical Research 102, 5753–5766.

McWilliams, J.C., Danabasoglu, G., Gent, P.R., 1996. Tracer budgets in the warm water sphere. Tellus 48, 179–192.

Nurser, A.J.G., Marsh, R., Williams, R.G., 1998. Diagnosing water mass formation from air-sea fluxes and surface mixing. Journal of Physical Oceanography, submitted.

Speer, K., Tziperman, E., 1992. Rates of water mass formation in the North Atlantic Ocean. Journal of Physical Oceanography, 22 93–104.

Speer, K.G., Isemer, H.-J., Biastoch, A., 1995. Water mass formation from revised COADS data. Journal of Physical Oceanography, 25, 2444–2457.

Speer, K.G., 1997. A note on average cross-isopycnal mixing in the North Atlantic Ocean. Deep-Sea Research I 44, 1981–1990.

Stommel, H., 1979. Determination of water mass properties of water pumped down from the Ekman layer to the geostrophic flow below. Proceedings of the National Academy of Sciences of the USA. 76, 3051–3055.

Tandon, A., Garrett, C., 1997. Water mass formation from thermodynamics: a framework for examining compatibility with dynamics. WOCE newsletter #28.

Walin, G., 1982. On the relation between sea-surface heat flow and thermal circulation in the ocean. Tellus 34, 187–195.

Williams, R.G., Spall, M.A., Marshall, J.C., 1995. Does Stommel's mixed layer demon work? Journal of Physical Oceanography 25, 3089–3102.